ChemPhysChem

Chemistry Europe
European Chemical Societies Publishing

Reprint

WILEY-VCH

Polymorphism of Amyloid Fibrils Induced by Catalytic Seeding: A Vibrational Circular Dichroism Study

Monika Krupová,[a, b] Jiří Kessler,[a] and Petr Bouř*[a]

Amyloidal protein fibrils occur in many biological events, but their formation and structural variability are understood rather poorly. We systematically explore fibril polymorphism for polyglutamic acid (PGA), insulin and hen egg white lysozyme. The fibrils were grown in the presence of "seeds", that is fibrils of the same or different protein. The seeds in concentrations higher than about 5% of the total protein amount fully determined the structure of the final fibrils. Fibril structure was monitored by vibrational circular dichroism (VCD) spectroscopy and other techniques. The VCD shapes significantly differ for different fibril samples. Infrared (IR) and VCD spectra of PGA were also simulated using density functional theory (DFT) and a periodic model. The simulation provides excellent basis for data interpretation and reveals that the spectral shapes and signs depend both on fibril length and twist. The understanding of fibril formation and interactions may facilitate medical treatment of protein misfolding diseases in the future.

1. Introduction

Fibrous protein aggregates are intensively studied as they occur in a of variety neurodegenerative conditions, such as Alzheimer's, Parkinson's, Huntington's disease or prion encephalopathies.[1] Also cell loss, vascular damage, and dementia were linked to fibril deposition in the living cells.[2] Unwanted fibril formation also deteriorates stability of some peptide therapeutics.[3] Understanding the factors affecting fibril growth, structure and interactions on the molecular level can thus in a final effect lead to better diagnostic methods, prevention and medical treatment. Many molecular properties can be conveniently pursued *in vitro*, where amyloidal fibrils can be prepared from a wide range of proteins and shorter peptides.[4]

The growth of amyloid fibrils is a slow and complicated process, not fully understood at the atomic level. Typically, fibril formation is characterized by a sigmoidal kinetic curve; the growth accelerates when first fibrils are formed.[5] The process can be speeded up by "seeding" using condensation nuclei, typically consisting of fibrils of the same protein.[6] The growth is slowed down at the end, when the fibrils "maturate". Typically, they become longer and/or denser. Even mature fibrils can change structure if put in a different environment. An illustrious example is insulin, forming left- or right-handed twisted fibrils, depending on pH.[7]

For a given environment different polymorphic fibrils can be formed according to initial nucleation mechanism. This can be illustrated on hen egg-white lysozyme (HEWL). The polymorph grown from non-seeded solutions exhibited a negative vibrational circular dichroism (VCD) in the amide I region, with the dissymmetry factor (g, VCD to absorption ratio) of about 10^{-3}. The seeds provided fibrils with positive and much bigger VCD signal with $g \sim 10^{-2}$.[8] Large g-factors are typically explained by tighter packing of the peptide strands, more regular and larger-scale crystal-like order, and stronger coupling of the carbonyl chromophores.[,9a,10] Similar polymorphism due to the seeding was occasionally observed also in other experiments.[7c,11]

Apart of the protein aggregates, fibrillations of synthetic gelators have been reported, exhibiting very similar VCD patterns.[12] Latest research on this field thus suggests that principles between chiral molecules forming fibril-like structures are rather general, and the interest exceeds protein or medical chemistry, with applications in molecular science, bioinformatics and industry.[13]

In the present work, we explore the effect of a homogeneous seeding with the same protein, and a heterogeneous seeding using fibrils of a different protein. Model systems involve poly L- and D-glutamic acid (PLGA and PDGA, respectively), HEWL and recombinant human insulin. In all cases, the seeding significantly accelerated the fibril formation and different preparation procedures provided different VCD shapes indicating structural differences. This is consistent with *in vivo* observations of the amyloidogenesis, significantly dependent on protein-protein interactions including cross-seeding.[14]

Chiroptical spectroscopic methods represent relatively simple and reliable tools for protein studies. In particular VCD spectral shapes and intensities are extremely sensitive to fibril structure.[7a,b,9c–e,10b,15] Experimentally accessible region usually

[a] M. Krupová, Dr. J. Kessler, Prof. P. Bouř
Institute of Organic Chemistry and Biochemistry
Academy of Sciences
Flemingovo náměstí 2, 16610 Prague, Czech Republic
E-mail: bour@uochb.cas.cz
[b] M. Krupová
Faculty of Mathematics and Physics
Charles University
Ke Karlovu 3, 12116, Prague 2, Czech Republic

Supporting information for this article is available on the WWW under https://doi.org/10.1002/cphc.202000797Supporting information for this article is available on the WWW under https://doi.org/10.1002/cphc.202000797

comprises amide I (largely C=O stretching around 1650 cm^{-1}) and amide II (C–N stretching combined with NH or ND bending, around 1535 cm^{-1} in H_2O and 1450 cm^{-1} in D_2O) vibrations.[9c,d,15d,16] Fibrils' *g*-factors ($\sim 10^{-4}$–10^{-2}) are usually much larger than for native (monomer) protein solutions or any other chiral organic molecules (typically 10^{-5}–10^{-4}).[17] The strength of the VCD signal significantly facilitates the measurement, otherwise requiring many hours of accumulation.

As shown below, VCD sensitivity to the fibril morphology has been confirmed in our experiments. For example, seeding of PLGA with itself and with enantiomeric PDGA provided PLGA fibrils of opposite VCD signs. Such events are sometimes referred to as the "sergeants-and-soldiers" principle, where the system chirality is determined by a relatively minor component.[18] Also the structure of HEWL and insulin fibrils is found to be quite sensitive to the initial seeding.

Various computational schemes were proposed to link the VCD pattern to the fibril structure in the past. The transition dipole coupling (TDC) model where the amide chromophores are represented by point dipoles provided basic VCD intensity shapes for stacked and twisted β-sheet planes[10a,19] or more complex systems.[9a] All-atomic simulations based on the density functional theory (DFT) force fields could be applied to smaller β-sheet like systems to reproduce finer features, such as effect of the isotopic editing.[10c,15h] The DFT/*ab initio* force fields can be extended to fairly large proteins using the Cartesian-coordinate based tensor transfer (CCT)[15g,20] or CCT combined with TDC.[21] The all-atomic DFT computations, however, are significantly limited by the diagonalization of the force field, currently practical only for systems with less than about 10000 atoms.[20b] The modeling thus may miss some effects coming from the large fibril size. At the present study, we use a regular periodic model applicable for PGA, to extend the DFT simulations further. The model allowed us to assign observed transitions and investigate the dependence of the spectra on the length and twist of fibril threads.

The VCD data are completed by transmission electron microscopy (TEM) images, confirming different fibril morphology. As an alternate spectroscopic probe, we use circularly polarized luminescence (CPL) induced in achiral lanthanide compounds. Lately, we found that a Raman optical activity (ROA) spectrometer can be conveniently used to measure CPL, and that the signal is very sensitive to the environment of the lanthanide ion or a lanthanide complex.[8,22] While VCD is also sensitive to the longer-range ordering, induced CPL senses the structure more locally, and thus provides convenient complementary information.

The data indicate that the sergeants-and-soldiers effect is quite common in the fibril formation. Although a full understanding at the atomic level may require further effort in the future, we believe that the findings are useful for analyses and manipulations of the fibrils in chemistry and biology.

2. Results and Discussion

2.1. PGA Solution, Fibrils, and Effect of Seeding

IR and VCD spectra of PLGA sodium salt solution where the peptide is in a monomer form are plotted in Figure 1, top. Two C=O stretching bands are present, one at 1648 cm^{-1}, of the amide I' vibration, and another at 1566 cm^{-1}, out of phase vibration of the COO^- group. (As usual, the apostrophe in amide I' etc. indicates a deuterated sample.) The other two strong bands belong to amide II' (1447 cm^{-1}) and in phase COO^- C=O stretching (1407 cm^{-1}) vibrations. The experimental spectra are consistent with previous experiments;[23] the amide I' VCD shape suggests that the monomer exists in an disordered conformation, partially adopting polyproline II-like helix.[24] The PDGA enantiomer provides VCD of nearly opposite sign (Figure S1 in the Supporting Information), confirming a good optical purity of the samples. The normal mode and conformation assignment could be also verified by the comparison to the simulated spectra of the rigid pentamer (Figure S2). The experimental VCD couplet at 1667(+)/1640(−) cm^{-1} is well-reproduced by the calculation, but at higher frequencies (1704/1690 cm^{-1}). The experimental *g*-factor ($\sim 1\times10^{-4}$) is much lower than calculated ($>1\times10^{-3}$). This is a consequence of the model rigidity, and modeling of all aspects of PGA monomer spectra goes beyond the scope of the present study.

The spontaneously grown fibrils at low pH produce quite different spectra (Figure 1, middle), details of which were analyzed previously.[9d,15g] The C=O COOD stretching IR band at 1730 cm^{-1} of the side chains produces a fairly strong VCD couplet 1740(−)/1725(+) cm^{-1}, although at this scale it appears relatively small against the dominant amide I' signal. The amide I' vibration produces two IR bands (1640 and 1599 cm^{-1}), which could be linked to variously-polarized β-sheet modes.[10a,15g,19] The strongest positive VCD band occurs at 1600 cm^{-1}, $g\sim3\times10^{-3}$ (cf. Table S1 summarizing the *g*-factors). The amide II' vibrations also generate more IR bands (1465, 1450 (shoulder)

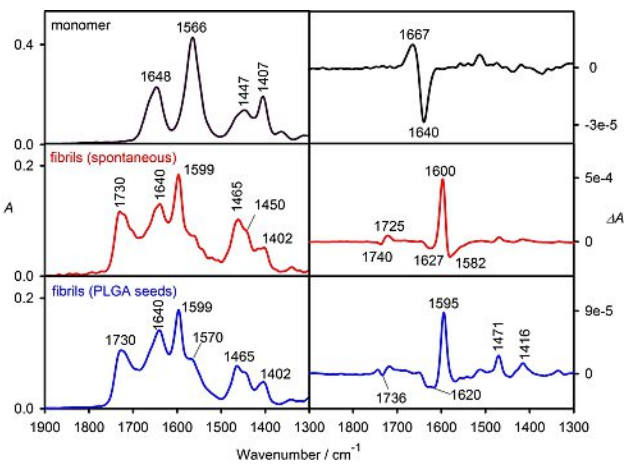

Figure 1. PLGA IR (*A*) and VCD (*ΔA*) spectra, monomer PLGA ion in sodium salt solution (pH ~ 7), fibrils grown at pH ~ 4.3 spontaneously, and using PLGA seeds.

and 1402 cm^{-1}), but relatively weak VCD at this scale. As shown in Figures S3–S4, PDGA fibrils give about opposite VCD sign patterns if compared to PLGA; the amide I′ absolute magnitude is smaller and also the amide II′ signal is not only opposite, but also slightly distorted. This corresponds to differences in molecular weight distribution, and was also observed previously.[9d]

PLGA fibrils seeded by PLGA (Figure 1, bottom) give similar but not the same spectra as the spontaneous ones. Relative IR intensities of the amide I′ bands differ only in a minor way. In VCD, the COOD signal around 1736 cm^{-1} adopts a three-sign w-shape, the main peak shifts to 1595 cm^{-1}, and minor differences occur in the negative bands around 1620 and 1680 cm^{-1}. The amide II′ bands, such as those at 1471 and 1416 cm^{-1}, become more visible and more comparable with the amide I′ intensity. The *g*-factor at 1595 cm^{-1} drops down to 5×10^{-4}, about six times less compared to the spontaneous case. We interpret this as a sign of "imperfect" fibrils, structure of which is far from the ideal β_2-form crystal arrangement.[25] In the accelerated growth initiated by the seeds either shorter or less-ordered condensates are formed, perhaps closer to the less compact β_1 PLGA form.[26]

2.2. Heterogeneous Seeding of PLGA

Even larger changes are obtained with seeds of a different compound. Seeds from the enantiomeric PDGA (Figure 2, top) cause sign flip of the main 1597 cm^{-1} VCD band compared to the homogeneous seeding by PLGA or spontaneous case, while IR remains about the same. The *g*-factor in absolute value is little bit smaller than for the PLGA seeds, 3×10^{-4}. The COOD signals (1741/1727 cm^{-1}) are opposite to the spontaneous case, but amide II′ VCD band signs are the same (Figure 1). The similarity of IR with the PLGA seeded sample suggests again that imperfect fibrils are formed, with a very similar secondary structure. However, the PDGA seeds impose their chirality and an effective macroscopic twist reflected in the amide I′ and COOD bands is opposite. The existence of fibrils of opposite twist has been observed for insulin, where, however, the twist was controlled by pH.[7a,b,15e]

Seeding PLGA by HEWL (Figure 2, middle) does not change the basic spontaneous fibril VCD pattern, but causes many other changes. The *g*-factor (4×10^{-4}) is smaller, and the VCD shape of the COOD stretching is nearly inverted. Finally, the insulin seeds (Figure 2, bottom) do not seem to interfere much with the growth of PGA fibrils, and IR and VCD patterns are very close to the spontaneous case. Only the *g*-factor of 22×10^{-4} is slightly smaller (cf. Table S1).

2.3. HEWL and Insulin Fibrils

Properties of fibrils of these natural proteins depend on the character of the seeds as well. IR and VCD spectra of native HEWL and insulin (Figure S5) are consistent with previous measurements[7a,15e,27] and computational modeling.[20b] The maximal *g*-factors are 2.1×10^{-5} (HEWL) and 4.4×10^{-5} (insulin).

In Figure 3 IR and VCD spectra of HEWL fibrils prepared by five seeding procedures (spontaneous, HEWL, insulin, PLGA and PDGA seeds) are compared. The spontaneous and HEWL cases were already reported in ref. [8], and give VCD patterns of approximately opposite signs. Unlike for PLGA, however, the spontaneous procedure (producing $g=4\times10^{-4}$) does not lead to the highest *g*-factor. This was achieved by the HEWL seeds ($g=39\times10^{-4}$). The insulin, PLGA and PDGA seeds gave lower *g*-factors (18×10^{-4}, 14×10^{-4} and 9×10^{-4}, respectively). All seeds also produced "reversed" fibrils, with a positive main amide I′

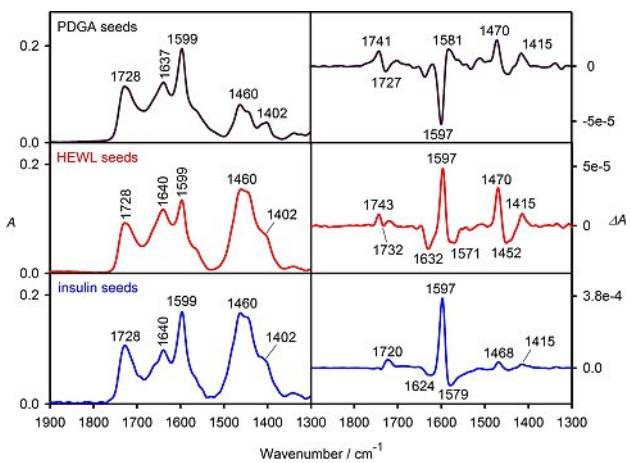

Figure 2. IR and VCD spectra of PLGA fibrils seeded by fibrils of different peptides, PDGA, HEWL and insulin.

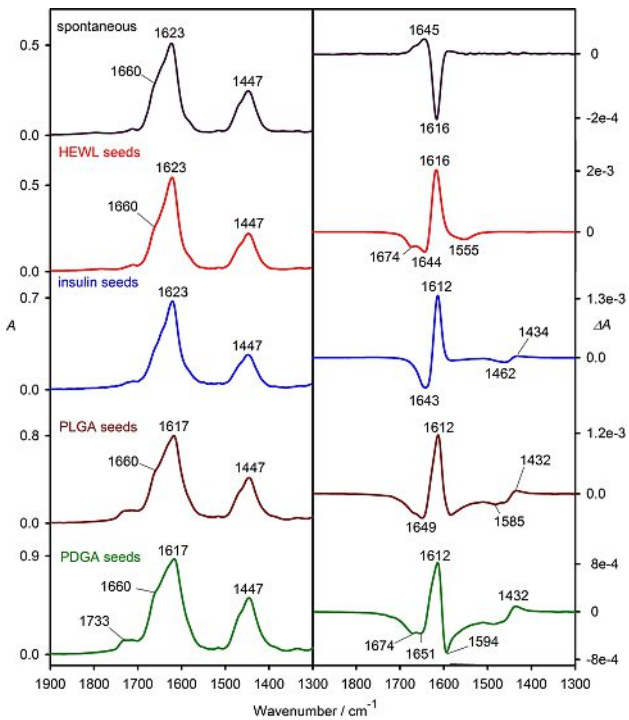

Figure 3. IR and VCD of HEWL fibrils, prepared with five seeding procedures (the spontaneous and HEWL cases were already reported in ref. [8]).

band, if compared to the spontaneous case. We may speculate that rather than due to a specific structure of the seeds, at least in this case, the reversed fibrils are formed due to the kinetic preference. Only during the spontaneous process, thermodynamically more stable "normal" fibrils are formed.

Slight differences in the amide I' IR band (~1700–1580 cm^{-1}) indicate structural changes related to different coupling of the amide chromophores.[19,28] The amide II' band signals appear similar, and occasional differences might be affected by an incomplete D/H exchange. The amide I' splitting (maximum at 1623 cm^{-1}, shoulder at 1660 cm^{-1}) indicates a high β-sheet content, as for PLGA. Insulin-seeded spectral shapes are probably most distinctly different from the others. For example, the amide IC IR band (1623 cm^{-1}) is quite sharp, and a couplet (−/+) dominates amide I' VCD, instead of a split signal around 1643 cm^{-1}. This is consistent with previous observations, where the kinetics of HEWL fibrillogenesis significantly depended on the environment, for which interaction of amino acid side chains appeared responsible.[29] It is interesting that minor differences are also caused by the PLGA/PDGA alteration. PLGA and PDGA have the same side chains, therefore the fibril structure must be sensitive also to finer interactions or a longer-range order. Because of the higher *g*-factors due to the seeding (Table S1), we may suppose that the seeding reverses the twist of HEWL fibrils and makes them more compact.

IR and VCD spectra of insulin fibrils prepared with different seeding are plotted in Figure 4, and show a unique behavior again. The spontaneous growth produces VCD dominated by amide I' bands, with negative minima at 1674 and 1659 cm^{-1} and a positive maximum at 1615 cm^{-1}, $g = 11 \times 10^{-4}$. When seeded by itself, the minima merge into a negative VCD band at 1647 cm^{-1} and the couplet becomes more balanced with $g = 9 \times 10^{-4}$. However, the other HEWL, PLGA and PDGA seeds produce approximately opposite amide I' VCD patterns, with a negative signal at 1609–1619 cm^{-1}. Smaller *g*-factors of 3×10^{-4}(HEWL and PLGA) and 4×10^{-4} (PDGA) may mean that the fibrils are less ordered than in the case of homogeneous seeding or spontaneous growth. Similarly as for HEWL, the differences in insulin fibril structure may be caused by kinetics factors. In fact, respect insulin follows the same pattern as HEWL, that is homogeneous seeding "improves" fibril structure, while heterogeneous one speeds up the formation and the fibril structure is more chaotic. Interestingly, PLGA and PDGA produced similar HEWL fibrils, but greater differences are visible in the insulin VCD spectrum.

Thus, although insulin seeds speed up formation of insulin fibrils, they do not significantly change VCD, and supposedly the macroscopic structure. The near reversion of the VCD pattern through the HEWL seeds suggests that already the "macroscopic chirality" (as reflected by VCD) may be determined in the initial stages of the fibrillation.

2.4. Induced CPL and TEM Images

Induced lanthanide CPL has been previously found sensitive to formation of the fibrils.[8] The Eu^{3+} ion is supposed to interact strongly with the carboxyl residue and its chirality is determined by the closest environment, perturbing *f-f* transitions of the lanthanide.[22b,30] Indeed, monomer and fibrillar PLGA give different CPL patterns around the 1900 cm^{-1} (592 nm) $^5D_0 \rightarrow {}^7F_1$ europium (III) band (Figure 5). Total (unpolarized) luminescence is not affected, and the $^5D_0 \rightarrow {}^7F_0$ transition at 1530 cm^{-1} (579 nm) does not generate induced CPL. Unlike for VCD, however, all seeding procedures provide the same CPL spectra. Only minor CPL differences are also visible for seeding with HEWL and insulin (Figure S6). We can therefore conclude that

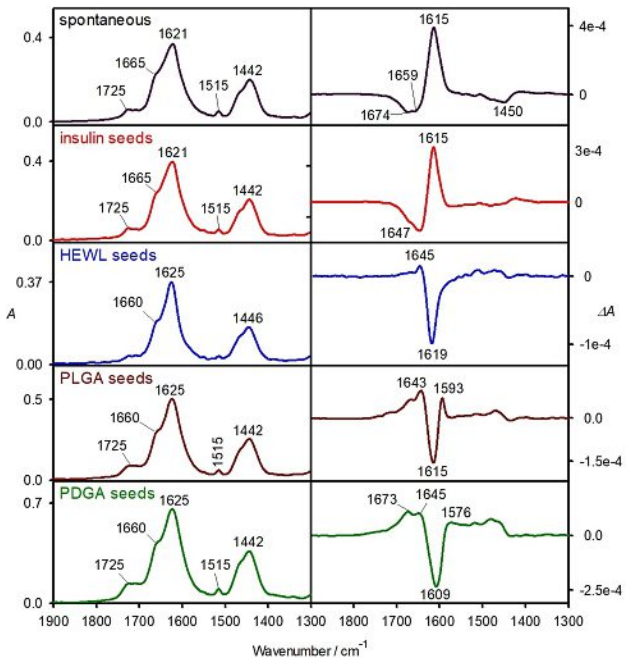

Figure 4. IR and VCD of insulin fibrils, prepared with five seeding procedures.

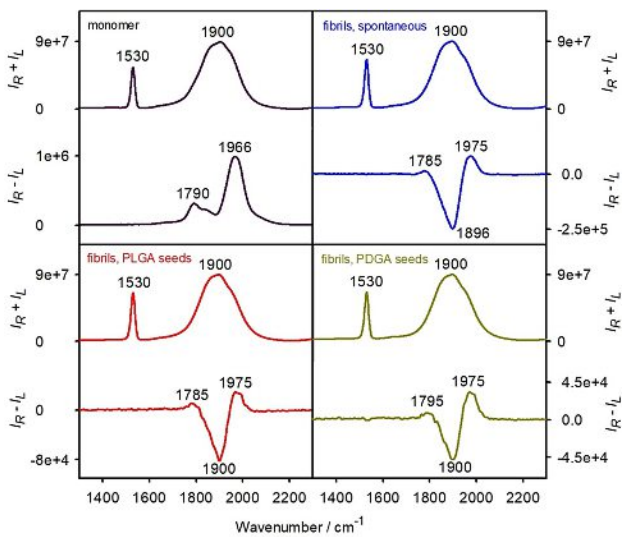

Figure 5. Total ($I_R + I_L$) and circular polarized ($I_R - I_L$) luminescence of $EuCl_3$ in the presence of PLGA in a form of monomer, spontaneous, PLGA and PDGA seeded fibrils. Shift from the 532 nm excitation is on the x-axis.

CPL and IR provide similar information on the local structure of the fibrils, whereas a more macroscopic arrangement, such as fibril length and twist, is better reflected by VCD.[7a] Similar results with a bigger CPL/TL ratio ($\sim 10^{-3}$–10^{-2}) were obtained with the $Na_3[Eu(DPA)_3]$ complex as a luminescence probe; however, the results are difficult to interpret in terms of the structure and not analyzed further.

The TEM images of the spontaneous and variously seeded fibrils (Figure S7) confirm that the structural differences indicated by the spectroscopies are connected to the macroscopic morphology. Unfortunately, the resolution and the number of reproducible differences are rather low, and detailed comparison to VCD/absorption spectral features is not possible.

2.5. Simulated vs. Experimental VCD Spectra of PLGA Fibrils

VCD shapes seem to be the most sensitive indicators of the fibril structure. The combined (DFT/TDC) periodic model provides at least qualitative understanding of the link between the structure and spectral shapes. For a hexamer and fibril twist $\varphi = 2°$ per two amide units, the simulated IR and VCD spectra are compared in Figure 6. The computation well reproduces the basic three-band IR pattern, of COOD carbonyl stretching and two amide I′ bands. As usual, computed IR band positions (1740/1671/1634 cm^{-1}) are slightly higher than in experiment (1730/1640/1599 cm^{-1}) because of the DFT error, incomplete solvent model, and anharmonic effects.[31] In VCD, the model correctly predicts the (−)/(+) couplet due to the COOD carbonyl stretching (computed at 1751/1741 cm^{-1}, experimentally 1740/1725 cm^{-1}). The simulated g-factor of ($\sim 1 \times 10^{-4}$) is smaller than in the experiment ($\sim 4 \times 10^{-4}$). The simulated amide I′ VCD provides negative 1675 cm^{-1} and positive 1638 cm^{-1} bands that can be associated with the experimental ones at 1627 and 1596 cm^{-1}. The experimental negative signal at 1582 cm^{-1} is not reproduced. Also the simulated amide I′ $g = 1 \times 10^{-4}$ is much smaller than in experiment (3×10^{-3}), which most probably reflects limited size of our model.

The model also allows us to estimate the dependence of VCD intensities on the twist. This is shown in Figure 7, where IR and VCD spectra for three twist angles were simulated. While IR does not significantly depend on the twist, VCD signal is smallest for $\varphi = 0°$. For $\varphi = 2°$ and $\varphi = -2°$ approximately opposite VCD patterns are obtained, both for the COOD and amide I′ signal. This can be explained by the dominance of the "macroscopic" chirality, reflected in the through-space coupling

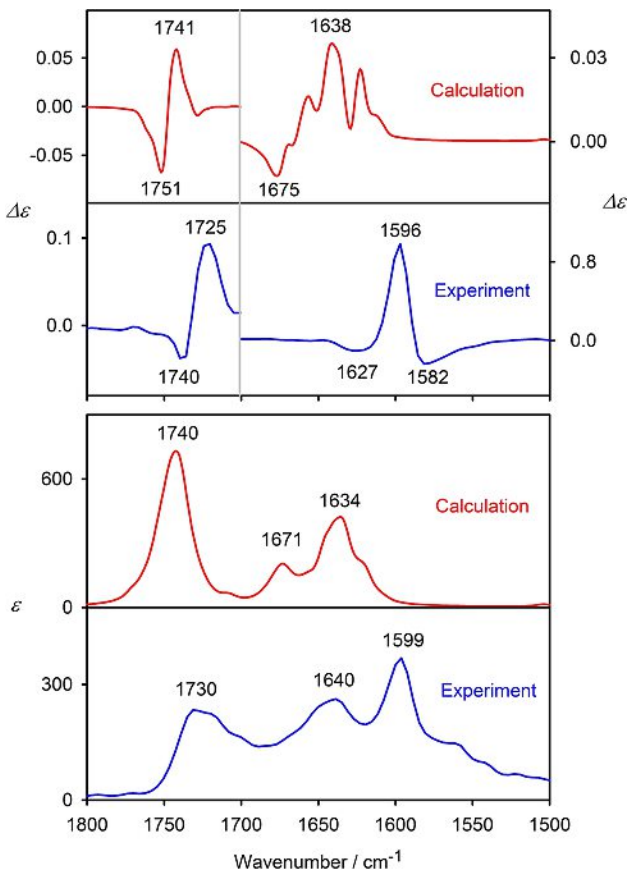

Figure 6. Calculated and experimental VCD and IR spectra of PLGA fibrils. Simulations are for the twist $\varphi = 2°$ and length $N = 6$, experiment for spontaneous fibrils.

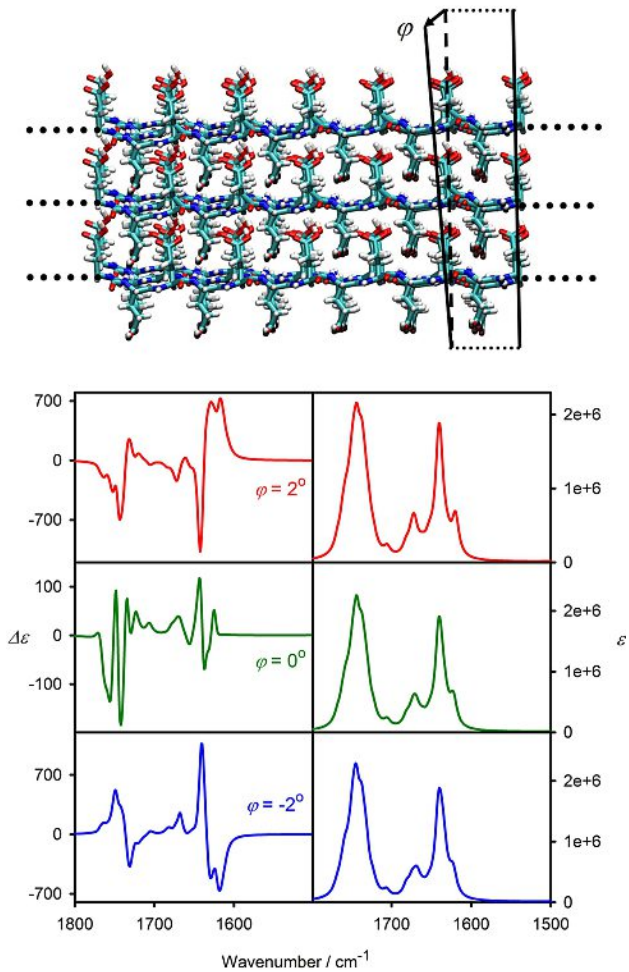

Figure 7. PLGA fibril VCD and IR spectra simulated for the three values of the twist φ. The length was constant ($N = 135$).

of electric transition dipole moments.[9a,10a,21] The relation of the VCD sign to the fibrils' twist has been experimentally proven for insulin.[7a,15e] For our experiments the microscopic images have resolution too low to recognize the twist.

The VCD sign depends on fibril length as well, which can potentially interfere with the twist dependence. In Figure 8 VCD spectra for $N=45$, 84 and 135 were simulated. Clearly, the shortest and longest systems provide opposite signs. Qualitatively, this dependence can be understood by an analysis of the geometry of the transition electric dipole moments responsible for the VCD intensity as indicated at the left-hand side of the figure. For the regular model and a non-zero twist the VCD patterns repeat after certain length, due to the constructive and destructive coupling of the dipoles.

The model thus suggests that the regular crystal-like structure of the fibrils enables coherent vibrations of the amide groups, reflected as a strong VCD signal. It should be nevertheless said that these longer-range interactions and coupling do not stabilize fibril geometry in any way. In fact, the sensitivity to the seeding suggests that more local interactions between amino acid residues and peptide chains already determine it in initial stages of the growth.

In experiment, the length-dependence of VCD may not be as important as the role of the twist, because a longer-range coupling present in the model may be impossible due to structural irregularities. Nevertheless, we believe that the relation between fibril length and VCD sign should also be taken into account while interpreting the experimental data. As far as we know this factor and its effect on VCD signs was ignored in previous literature.

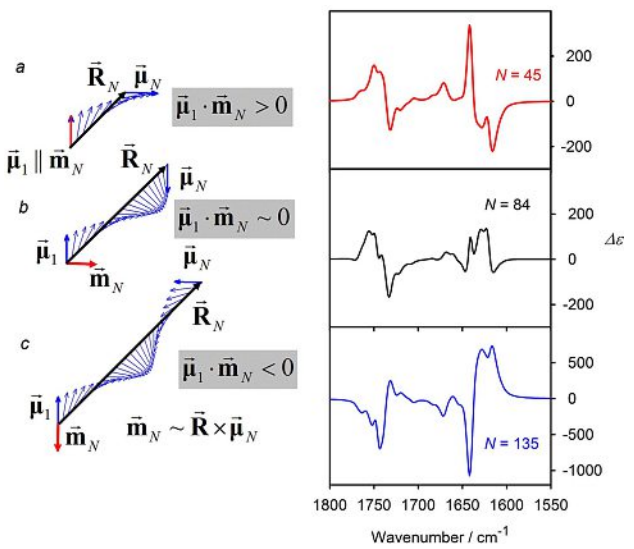

Figure 8. On the right: Simulated dependence of PLGA fibril VCD spectra on the length for a constant $\varphi = 2°$ twist, N is the number of two amide elementary units. $N=45$ thus corresponds to the total twist of 90° between amide groups at the beginning and the end of the thread, etc. On the left, geometries of the terminal electric transition dipole moments ($\boldsymbol{\mu}_1$, $\boldsymbol{\mu}_N$) providing the biggest rotational strength are schematically indicated, $\mathbf{R}_N$ is the distance vector. a) for $N=45$ the $\boldsymbol{\mu}_1$ and $\boldsymbol{\mu}_N$ are about perpendicular and $\boldsymbol{\mu}_N$ generates a magnetic moment $\vec{\mathbf{m}}_N \sim \vec{\mathbf{R}}_N \times \vec{\boldsymbol{\mu}}_N$ (with the origin on $\boldsymbol{\mu}_1$) parallel to $\boldsymbol{\mu}_1$, resulting in a positive rotational strength $\vec{\boldsymbol{\mu}}_1 \cdot \vec{\mathbf{m}}_N$. b) for N close to 90 $\boldsymbol{\mu}_1$ and $\boldsymbol{\mu}_N$ are pointing to opposite directions and rotational strength is close to zero. c) for $N \sim 135$ $\boldsymbol{\mu}_1$ and $\boldsymbol{\mu}_N$ are perpendicular again, but rotational strength is opposite to case a).

3. Conclusions

For the PLGA and PDGA polypeptides and HEWL and insulin proteins we systematically investigated the outcome when the fibrils were grown without and with presence of the nucleation seeds. The seeds significantly affected the structure of the resultant fibrils as could be monitored by the IR, VCD, and induced lanthanide CPL spectra. The VCD technique appeared the most sensitive; for example, the signal strength of the amide I' vibration changed within several orders of magnitude and even the sign could be flipped. The results confirm the importance of the "sergeants-and-soldiers" mechanism during the initial stage of the fibrillation, when the structure of the product in the fast-growing stage is already determined. We may conclude that various polymorphic fibrils have very similar "local" secondary structure, largely β-sheet, seen by IR and CPL spectra, but differ in length/twist/macroscopic arrangement and chirality reflected in VCD. The DFT modeling provided band assignment and could reproduce basic spectral features observed experimentally. It thus casted some light on the link between the structure and VCD pattern, although more realistic models are needed in the future to fully understand fibril behavior and interactions. We believe that the combination of the theory and VCD experiments is an excellent means for fibril studies. In the future it may become useful for the diagnosis and treatment of the protein misfolding diseases, and other applications.

Experimental Section

Fibril Preparation

HEWL, human recombinant insulin and both enantiomers of sodium salt of polyglutamic acid (PGA, molecular weight 15–50 kDa) were obtained from Sigma-Aldrich. To avoid interference of water signal in the wavenumber region of interest (1500–1800 cm^{-1}) for VCD and absorption (IR) measurement, the fibrils were repeatedly dissolved in D_2O and lyophilized. The fibrils were prepared according to procedures suggested previously.[9c,d] To aqueous solution of HEWL (100 mg/mL) 1 M solution of DCl was added so that resultant pH = 2, and the fibrils were incubated at 60 °C for 48 h. For insulin, the concentration was 40 mg/mL, pH was also adjusted by 1 M DCl to 2, and the incubation ran at 65 °C for 24 h. In case of PGA, aqueous solutions of 15 mg/mL and pH 4.3 were incubated directly at 65 °C for 48 h. The seeds were prepared by ultrasonication of mature fibril solutions for 1 hour and added to the starting protein solutions in the default 1:9 seed to protein ratio. We chose the same (48 h) incubation period for all studied fibrils before measurement, to suppress any significant time-dependence of the data.[7a,b,9d,e] Note that minor changes in fibril VCD spectra or structure cannot be excluded even after a longer time.[15j] According to the tests (Figure S8) ratios above 1:19 (5%) already start to completely determine the outcome of the fibril growth.

Vibrational Spectra

IR absorption and VCD spectra of aggregated samples were measured on a ChiralIR instrument (BioTools), using BaF_2 cell of 50 μm (PGA) and 15 μm (insulin and HEWL) optical path lengths, 4 cm diameter, teflon spacer, 8 cm^{-1} resolution, 6 blocks of 2048 scans, and 2 h total accumulation time. D_2O spectra were subtracted as a baseline, no additional sealing (grease) was applied, and the cell was rotated during the measurements. We did not observe a significant dependence of VCD on sample rotation; example of spectra collected with and without rotation of the sample around the beam axis is in Figure S9.

For non-aggregated proteins, to increase VCD signal to noise ratio, the concentration of PGA was 45 mg/ml while for HEWL and insulin it was the same as for the fibrils; the optical path length was 25 μm. HEWL and PGA were dissolved in pure D_2O, for insulin pD was changed to two to increase its solubility. The accumulation time was 16 h.

All experiments were performed at least three times and the average is reported. Each of the triplicate included a new preparation of the incubated solution, pH adjustment, 48 h incubation, and transfer of the fibrils to the spectrometer cell. Examples of individual measurements for HEWL together with instrumental noise can be seen in Figure S10.

Induced CPL Spectra

Solutions of mature amyloid fibrils were mixed with either $EuCl_3$ (PLGA and PDGA) or $Na_3[Eu(DPA)_3]$ (for HEWL and insulin; DPA = pyridine-2,6-dicarboxylic acid), to final concentration of the Eu^{3+} luminophore of 1 mM. CPL and total luminescence (TL) spectra were measured on a ROA instrument ChiralRAMAN-2x (BioTools) using 532 nm laser excitation, 500 mW laser power, 2-second illumination time and 1-hour acquisition. For control, we also measured ROA spectra of native proteins with 16-hour acquisition time and 45 mg/ml PGA concentration, for HEWL and insulin the concentration was the same as for the fibrils. The ROA measurements were performed in water (for insulin at pH 2, 16 h acquisition, otherwise same conditions as for CPL); they were consistent with previously published results.[32]

Transmission Electron Microscopy

Amyloid fibril solutions were diluted 10× while maintaining pH at 4.3 (polyglutamic acids) or 2.0 (HEWL, insulin), then 10 μL were deposited on a carbon-coated grid and stained with 4 wt% phosphotungstic acid. The images were acquired on a JEOL JEM-1200EX microscope.

Density Functional Theory Computations

The computations for PLGA were performed at the B3LYP[33]/6–31G**/CPCM[34] (H_2O) default level of theory using the Gaussian program[35] and our supplementary software.[36] To assign solution (random-structure) vibrations, IR and VCD spectra were simulated for a $(Glu_5)^{5-}$ ion, torsions of which were kept in the idealized polyproline II conformation.[37] The 6–31G** basis set enabled us to calculate relatively large fibril fragments; it also provided reasonable results in VCD modeling of larger peptides previously.[38] Only for $(Glu_5)^{5-}$ a bigger 6–31++G** basis set was used. For the fibrils, as in previous modelling,[15g] the geometry mimicked the crystal β_2 structure.[9d,25–26] Newly, a minor helical twist (−2, 0 and 2° per two amide residues) was arbitrarily introduced to idealized threads composed of 12 polypeptide chains. Note that twists bigger than 2 degrees lead to unrealistic distortion of the fibril thread, up to breaking of the covalent bonds in the peptide chain. On the other hand, smaller twists are regularly observed in peptide fibrils, including glutamic acid based peptides,[9e] bacterial protein binding proteins[39] and α-synuclein.[40]

Four chains were combined in three anti-parallel β-sheets, which were then stacked (144 amide groups in total). Except for the twist, the crystal parameters were used. The repeating unit thus comprised 24 amino acid residues. This "idealized" structure (N = 6 units) was optimized using the Gaussian program[35] and universal molecular mechanic force field (UFF);[41] for the periodic model non-optimized geometry was used. Vibrational parameters (force field, atomic polar and atomic axial tensor) obtained previously for a smaller fragment[15g] were transferred on the fibril model geometry using the Cartesian-coordinate based tensor transfer (CCT),[20a,42] and TDC corrections[21] between distant amode groups were added to the force field. The fragment (Figure S11) included interactions most important for C=O stretching VCD, such as neighboring amide-amide coupling, closest amide-amide and amide-COOD interactions between different peptide strands, etc.

For longer periodic PGA fibrils the DFT computations were extended using the crystal vibration methodology.[36] The Hamiltonian within the harmonic approximation can be written as

$$H = \frac{1}{2}\sum_{\lambda}\sum_{\alpha} m_{\lambda}\dot{x}^{*}_{\lambda\alpha}\dot{x}_{\lambda\alpha} + \frac{1}{2}\sum_{\lambda}\sum_{\mu}\sum_{\alpha}\sum_{\beta} x^{*}_{\lambda\alpha} f_{\lambda\alpha\mu\beta} x_{\mu\beta} \tag{1}$$

where m_λ is mass and $x_{\lambda\alpha}$ is α-coordinate ($\alpha = x$, y, or z) of atom λ, and $f_{\lambda\alpha,\mu\beta}$ is a force field (Hessian) element. As usual for periodic structures,[43] by a coordinate transformation the Hamiltonian can be further transformed to a sum of harmonic oscillators

$$H = \frac{1}{2}\sum_{q}\sum_{J_q}\left(\dot{Q}^2_{J_q} + \omega^2_{J_q} Q^2_{J_q}\right) \tag{2}$$

where q is the phonon mode and the index J_q goes over normal modes in the elementary cell. We neglected the end effects and simulated one-dimensional fibril thread. The atomic coordinates in an elementary unit J were expanded into the plane waves,

$$x^{(J)}_{\lambda\alpha} = \sum_{q=0}^{N-1} \exp\left(\frac{2\pi q J}{N} i\right) / \sqrt{N}\, X_{q,\lambda\alpha} \tag{3}$$

where $X_{q,\lambda\alpha}$ are the coordinates in the reference unit. The dynamic matrix is then

$$D_{q,\lambda\alpha,\mu\beta} = \sum_{J} f_{\lambda\alpha,\mu\beta} e^{i\frac{2\pi q}{N}J} \tag{4}$$

and the harmonic frequencies in (2) are obtained by the diagonalization

$$\omega^2_q \delta_{J_q J_q} = \sum_{\lambda\alpha}\sum_{\mu\beta} S^{*}_{q,\lambda\alpha J_q} D_{q,\lambda\alpha\mu\beta} S_{q,\mu\beta J_q} \tag{5}$$

where δ is the Kronecker delta and S is the Cartesian-normal mode transformation matrix. By this approach diagonalization of a large $3Nat \times 3Nat$ f-matrix in (1) is replaced by N diagonalizations (for each q) of $(3Nat/N)\times(3Nat/N)$ D matrices in Equation (5), which is much easier computational task.

The theoretical spectra were simulated using line intensities convoluted with Lorentzian bands of 10 cm^{-1} full width at half maximum. We model the carboxyl CO stretching and amide I′ regions only, because more delocalized amide II′ and other

vibrations are not compatible with the CCT model[42] and geometry restrictions used to simulate the twist.

Acknowledgements

This work was funded by the Grant Agency and Ministry of Education of the Czech Republic (grant numbers 18-05770S (PB), 20-10144S (JK), LM2018140, and CZ.02.1.01/0.0/0.0/16_019/0000729).

Conflict of Interest

The authors declare no conflict of interest.

Keywords: catalytic seeding · fibrous proteins · molecular modeling · protein folding · vibrational circular dichroism

[1] a) A. Aguzzi, T. O'Connor, *Nat Rev Drug Discov* **2010**, *9*, 237–248; b) F. Chiti, C. M. Dobson, *Annu. Rev. Biochem.* **2017**, *86*, 27–68; c) C. M. Dobson, *Semin. Cell Dev. Biol.* **2004**, *15*, 3–16.
[2] J. A. Hardy, G. A. Higgins, *Science* **1992**, *256*, 184–185.
[3] K. L. L. Zapadka, F. J. Becher, A. L. G. Santos, S. E. Jackson, *Interface Focus* **2017**, *7*, 20170030.
[4] a) M. Fandrich, M. A. Fletcher, C. M. Dobson, *Nature* **2001**, *410*, 165–166; b) J. Goers, S. E. Permyakov, E. A. Permyakov, V. N. Uversky, A. L. Fink, *Biochemistry* **2002**, *41*, 12546–12551; c) J. J. Lai, C. Zheng, D. H. Liang, Y. B. Huang, *Biomacromolecules* **2013**, *14*, 4515–4519; d) L. Tjernberg, W. Hosia, N. Bark, J. Thyberg, J. Johansson, *J. Biol. Chem.* **2002**, *277*, 43243–43246; e) A. Iyer, S. J. Roeters, V. Kogan, S. Woutersen, M. M. A. E. Claessens, V. Subramaniam, *J. Am. Chem. Soc.* **2017**, *139*, 15392–15400.
[5] a) J. E. Gillam, C. E. MacPhee, *J. Condens. Matter Phys.* **2013**, *25*, 373101; b) T. Hard, *J. Phys. Chem. Lett.* **2014**, *5*, 607–614; c) A. M. Morris, M. A. Watzky, R. G. Finke, *Bba-Proteins Proteom.* **2009**, *1794*, 375–397.
[6] a) J. D. Harper, P. T. Lansbury, *Annu. Rev. Biochem.* **1997**, *66*, 385–407; b) C. Soto, L. Anderes, S. Suardi, F. Cardone, J. Castilla, M. J. Frossard, S. Peano, P. Saa, L. Limido, M. Carbonatto, J. Ironside, J. M. Torres, M. Pocchiari, F. Tagliavini, *FEBS Lett.* **2005**, *579*, 638–642; c) C. Soto, G. P. Saborio, L. Anderes, *Trends Neurosci.* **2002**, *25*, 390–394.
[7] a) D. Kurouski, R. K. Dukor, X. Lu, L. A. Nafie, I. K. Lednev, *Chem. Commun.* **2012**, *48*, 2837–2839; b) D. Kurouski, X. F. Lu, L. Popova, W. Wan, M. Shanmugasundaram, G. Stubbs, R. K. Dukor, I. K. Lednev, L. A. Nafie, *J. Am. Chem. Soc.* **2014**, *136*, 2302–2312; c) T. Sneideris, D. Darguzis, A. Botyriute, M. Grigaliunas, R. Winter, V. Smirnovas, *PLoS One* **2015**, *10*, e0136602.
[8] M. Krupová, J. Kapitán, P. Bouř, *ACS Omega* **2019**, *4*, 1265–1271.
[9] a) J. Průša, P. Bouř, *Chirality* **2018**, *30*, 55–64; b) D. Kurouski, J. D. Handen, R. K. Dukor, L. A. Nafie, I. K. Lednev, *Chem. Commun.* **2015**, *51*, 89–92; c) S. Ma, X. Cao, M. Mak, A. Sadik, C. Walkner, T. B. Freedman, I. K. Lednev, R. K. Dukor, L. A. Nafie, *J. Am. Chem. Soc.* **2007**, *129*, 12364–12365; d) A. Fulara, A. Lakhani, S. Wójcik, H. Nieznańska, T. A. Keiderling, W. Dzwolak, *J. Phys. Chem. B* **2011**, *115*, 11010–11016; e) F. Tobias, T. A. Keiderling, *Langmuir* **2016**, *32*, 4653–4661.
[10] a) T. Measey, R. Schweitzer-Stenner, *J. Am. Chem. Soc.* **2011**, *133*, 1066–1076; b) W. R. W. Welch, T. A. Keiderling, J. Kubelka, *J. Phys. Chem. B* **2013**, *117*, 10359–10369; c) W. R. W. Welch, J. Kubelka, T. A. Keiderling, *J. Phys. Chem. B* **2013**, *117*, 10343–10358.
[11] a) H. A. Davies, C. F. Lee, L. Miller, L. N. Liu, J. Madine, *Int. J. Mol. Sci.* **2018**, *19*; b) A. K. Paravastu, I. Qahwash, R. D. Leapman, S. C. Meredith, R. Tycko, *Proc. Natl. Acad. Sci. USA* **2009**, *106*, 7443–7448; c) W. Surmacz-Chwedoruk, V. Babenko, R. Dec, P. Szymczak, W. Dzwolak, *Sci. Rep.* **2016**, *6*, 32022; d) J. Q. Ma, H. Komatsu, P. H. Axelsen, *Biophys. J.* **2014**, *106*, 680a.
[12] a) H. Sato, T. Yajima, A. Yamagishi, *Phys. Chem. Chem. Phys.* **2018**, *20*, 3210–3215; b) T. Yajima, E. Tabuchi, E. Nogami, A. Yamagishi, H. Sato, *RSC Adv.* **2015**, *5*, 80542–80547.
[13] X. Du, J. Zhou, J. Shi, B. Xu, *Chem. Rev.* **2015**, *115*, 13165–13307.
[14] a) C. Venegas, S. Kumar, B. S. Franklin, T. Dierkes, R. Brinkschulte, D. Tejera, A. Vieira-Saecker, S. Schwartz, F. Santarelli, M. P. Kummer, A. Griep, E. Gelpi, M. Beilharz, D. Riedel, D. T. Golenbock, M. Geyer, J. Walter, E. Latz, M. T. Heneka, *Nature* **2017**, *552*, 355–361; b) K. Lundmark, G. T. Westermark, A. Olsen, P. Westermark, *Proc. Natl. Acad. Sci. USA* **2005**, *102*, 6098–6102; c) T. L. Spires-Jones, J. Attems, D. R. Thal, *Acta Neuropathol.* **2017**, *134*, 187–205.
[15] a) X. F. Lu, H. G. Li, J. W. Nafie, T. Pazderka, M. Pazderková, R. K. Dukor, L. A. Nafie, *Appl. Spectrosc.* **2017**, *71*, 1117–1126; b) M. Pazderková, T. Pazderka, M. Shanmugasundaram, R. K. Dukor, I. K. Lednev, L. A. Nafie, *Chirality* **2017**, *29*, 469–475; c) M. Shanmugasundaram, D. Kurouski, W. Wan, G. Stubbs, R. K. Dukor, L. A. Nafie, I. K. Lednev, *J. Phys. Chem. B* **2015**, *119*, 8521–8525; d) D. Kurouski, K. Kar, R. Wetzel, R. K. Dukor, I. K. Lednev, L. A. Nafie, *FEBS Lett.* **2013**, *578*, 1638–1643; e) D. Kurouski, R. A. Lombardi, R. K. Dukor, I. K. Lednev, L. A. Nafie, *Chem. Commun.* **2010**, *46*, 7154–7156; f) E. Van de Vondel, P. Baatsen, R. Van Elzen, A. M. Lambeir, T. A. Keiderling, W. A. Herrebout, C. Johannessen, *Biochemistry* **2018**, *57*, 5989–5995; g) J. Kessler, T. A. Keiderling, P. Bouř, *J. Phys. Chem. B* **2014**, *118*, 6937–6945; h) H. Chi, W. R. W. Welch, J. Kubelka, T. A. Keiderling, *Biomacromolecules* **2013**, *14*, 3880–3891; i) W. Dzwolak, *Chirality* **2014**, *26*, 580–587; j) S. J. Roeters, M. Sawall, C. E. Eskildsen, M. R. Panman, G. Tordai, M. Koeman, K. Neymeyr, J. Jansen, A. K. Smilde, S. Woutersen, *Biophys. J.* **2020**, *119*, 87–98.
[16] V. Babenko, W. Dzwolak, *FEBS Lett.* **2013**, *587*, 625–630.
[17] a) T. A. Keiderling, *Chem. Rev.* **2020**, *120*, 3381–3419; b) M. Krupová, J. Kessler, P. Bouř, *ChemPlusChem* **2020**, *85* 561–575.
[18] a) L. J. Prins, P. Timmerman, D. N. Reinhoudt, *J. Am. Chem. Soc.* **2001**, *123*, 10153–10163; b) T. W. Anderson, J. K. M. Sanders, G. D. Pantoş, *Org. Biomol. Chem.* **2010**, *8*, 4274–4280.
[19] R. S. Stenner, *J. Phys. Chem. B* **2012**, *116*, 4141–4153.
[20] a) P. Bouř, J. Sopková, L. Bednárová, P. Maloň, T. A. Keiderling, *J. Comput. Chem.* **1997**, *18*, 646–659; b) J. Kessler, V. Andrushchenko, J. Kapitán, P. Bouř, *Phys. Chem. Chem. Phys.* **2018**, *20*, 4926–4935.
[21] J. Kubelka, J. Kim, P. Bouř, T. A. Keiderling, *Vib. Spectrosc.* **2006**, *42*, 63–73.
[22] a) T. Wu, J. Průša, J. Kessler, M. Dračínský, J. Valenta, P. Bouř, *Anal. Chem.* **2016**, *88*, 8878–8885; b) T. Wu, J. Kessler, P. Bouř, *Phys. Chem. Chem. Phys.* **2016**, *18*, 23803–23811; c) E. Brichtová, H. J. N. Vršková, J. Šebestík, P. Bouř, T. Wu, *Chem. Eur. J.* **2018**, *24*, 8664–8669; d) T. Wu, P. Bouř, V. Andrushchenko, *Sci. Rep.* **2019**, *9*, 1068.
[23] P. Novotná, M. Urbanová, *Chirality* **2015**, *27*, 965–972.
[24] R. K. Dukor, T. A. Keiderling, *Biopolymers* **1991**, *31*, 1747–1761.
[25] H. D. Keith, G. Giannoni, F. J. Padden, *Biopolymers* **1969**, *7*, 775–792.
[26] K. Itoh, B. M. Foxman, G. D. Fasman, *Biopolymers* **1976**, *15*, 419–455.
[27] a) T. A. Keiderling, B. Wang, M. Urbanová, P. Pančoška, R. K. Dukor, *Faraday Discuss.* **1994**, *99*, 263–286; b) A. Giugliarelli, P. Sassi, M. Paolantoni, A. Morresi, R. Dukor, L. Nafie, *J. Phys. Chem. B* **2013**, *117*, 2645–2652.
[28] a) R. Huang, V. Setnička, M. A. Etienne, J. Kim, J. Kubelka, R. P. Hammer, T. A. Keiderling, *J. Am. Chem. Soc.* **2007**, *129*, 13592–13603; b) V. Setnička, R. Huang, C. L. Thomas, M. A. Etienne, J. Kubelka, R. P. Hammer, T. A. Keiderling, *J. Am. Chem. Soc.* **2005**, *127*, 4992–4993.
[29] A. Cao, D. Hu, L. Lai, *Protein Sci.* **2004**, *13*, 319–324.
[30] K. Binnemans, *Coord. Chem. Rev.* **2015**, *295*, 1–45.
[31] a) P. Bouř, D. Michalík, J. Kapitán, *J. Chem. Phys.* **2005**, *122*, 144501; b) J. Kubelka, R. Huang, T. A. Keiderling, *J. Phys. Chem. B* **2005**, *109*, 8231–8243.
[32] a) J. Kessler, J. Kapitán, P. Bouř, *J. Phys. Chem. Lett.* **2015**, *6*, 3314–3319; b) S. Yamamoto, J. Kaminský, P. Bouř, *Anal. Chem.* **2012**, *84*, 2440–2451; c) I. H. McColl, E. W. Blanch, L. Hecht, N. R. Kallenbach, L. D. Barron, *J. Am. Chem. Soc.* **2004**, *126*, 5076–5077 ; d) L. Ashton, L. D. Barron, L. Hecht, J. Hyde, E. W. Blanch, *Analyst* **2007**, *132*, 468–479.
[33] A. D. Becke, *J. Chem. Phys.* **1993**, *98*, 5648–5652.
[34] M. Cossi, N. Rega, G. Scalmani, V. Barone, *J. Comput. Chem.* **2002**, *24*, 669–681.
[35] M. J. Frisch, G. W. Trucks, H. B. Schlegel, G. E. Scuseria, M. A. Robb, J. R. Cheeseman, G. Scalmani, V. Barone, G. A. Petersson, H. Nakatsuji, X. Li, M. Caricato, A. V. Marenich, J. Bloino, B. G. Janesko, R. Gomperts, B. Mennucci, H. P. Hratchian, J. V. Ortiz, A. F. Izmaylov, J. L. Sonnenberg, Williams, F. Ding, F. Lipparini, F. Egidi, J. Goings, B. Peng, A. Petrone, T. Henderson, D. Ranasinghe, V. G. Zakrzewski, J. Gao, N. Rega, G. Zheng, W. Liang, M. Hada, M. Ehara, K. Toyota, R. Fukuda, J. Hasegawa, M. Ishida, T. Nakajima, Y. Honda, O. Kitao, H. Nakai, T. Vreven, K. Throssell, J. A. Montgomery Jr., J. E. Peralta, F. Ogliaro, M. J. Bearpark, J. J. Heyd,

E. N. Brothers, K. N. Kudin, V. N. Staroverov, T. A. Keith, R. Kobayashi, J. Normand, K. Raghavachari, A. P. Rendell, J. C. Burant, S. S. Iyengar, J. Tomasi, M. Cossi, J. M. Millam, M. Klene, C. Adamo, R. Cammi, J. W. Ochterski, R. L. Martin, K. Morokuma, O. Farkas, J. B. Foresman, D. J. Fox, *Gaussian, Inc.*, Wallingford, CT, **2016**.
[36] P. Bouř, *Academy of Sciences*, Prague, **1997–2019**.
[37] T. E. Creighton, *Proteins: Structures and Molecular Properties*, 2nd ed., W. H. Freeman and Co., New York, **1993**.
[38] P. Bouř, T. A. Keiderling, *J. Chem. Phys.* **2003**, *119*, 11253–11262.
[39] a) J. Badger, J. M. Sauder, J. M. Adams, S. Antonysamy, K. Bain, M. G. Bergseid, S. G. Buchanan, M. D. Buchanan, Y. Batiyenko, J. A. Christopher, S. Emtage, A. Eroshkina, I. Feil, E. B. Furlong, K. S. Gajiwala, X. Gao, D. He, J. Hendle, A. Huber, K. Hoda, P. Kearins, C. Kissinger, B. Laubert, H. A. Lewis, J. Lin, K. Loomis, D. Lorimer, G. Louie, M. Maletic, C. D. Marsh, I. Miller, J. Molinari, H. J. Muller-Dieckmann, J. M. Newman, B. W. Noland, B. Pagarigan, F. Park, T. S. Peat, K. W. Post, S. Radojicic, A. Ramos, R. Romero, M. E. Rutter, W. E. Sanderson, K. D. Schwinn, J. Tresser, J. Winhoven, T. A. Wright, L. Wu, J. Xu, T. J. R. Harris, *Proteins* **2005**, *60*, 787–796; b) J. Kessler, S. Yamamoto, P. Bouř, *Phys. Chem. Chem. Phys.* **2017**, *19*, 13614–13621.
[40] B. Li, P. Ge, K. A. Murray, P. Sheth, M. Zhang, G. Nair, M. R. Sawaya, W. S. Shin, D. R. Boyer, S. Ye, D. S. Eisenberg, Z. H. Zhou, L. Jiang, *Nat. Commun.* **2018**, *9*, 3609.
[41] A. K. Rappe, C. J. Casewit, K. S. Colwell, W. A. Goddard III, W. M. Skiff, *J. Am. Chem. Soc.* **1992**, *114*, 10024–10035.
[42] S. Yamamoto, X. Li, K. Ruud, P. Bouř, *J. Chem. Theory Comput.* **2012**, *8*, 977–985.
[43] L. Piseri, G. Zerbi, *J. Mol. Spectrosc.* **1968**, *26*, 254–261.

Manuscript received: September 21, 2020
Revised manuscript received: October 16, 2020
Accepted manuscript online: October 20, 2020
Version of record online: November 23, 2020